

**SYNTHESIS AND CHARACTERIZATIONS OF  
VARIOUS METAL-BASED HALLOYSITE  
NANOCOMPOSITES FOR THE PHOTO-  
DEGRADATION OF LIQUID EPOXIDIZED  
NATURAL RUBBER**

**ABDULLAHI SHEHU SAAD**

**UNIVERSITI SAINS MALAYSIA**

**2024**

**SYNTHESIS AND CHARACTERIZATIONS OF  
VARIOUS METAL-BASED HALLOYSITE  
NANOCOMPOSITES FOR THE PHOTO-  
DEGRADATION OF LIQUID EPOXIDIZED  
NATURAL RUBBER**

by

**ABDULLAHI SHEHU SAAD**

**Thesis submitted in fulfilment of the requirements  
for the degree of  
Doctor of Philosophy**

**September 2024**

## ACKNOWLEDGEMENT

All thanks and gratitude go to Allah SWT for giving me the opportunity, sound health and endlessly help during my PhD journey. Special gratitude goes to our Noble Prophet Muhammad (Peace be Upon Him).

I would like to extend my heartfelt gratitude to my supervisor, Associate Professor Dr. Noor Hana Hanif Abu Bakar for her tireless guidance, mentorship, support, advice, and insightful comments, throughout the research journey. May ALLAH reward her abundantly and bless her family. I would like to sincerely thanks Dr. Anwar Iqbal and Dr. Nurul Hayati Yusof of the Malaysian Rubber Board, Engineering and Technology Division, Selangor, Sungai Buluh, Malaysia for support, especially GPC analysis.

I must thank all staff of the School of Chemical Sciences, Centre for Global Archaeological Research, School of Material (Engineering Campus), and School of Physics for their support, particularly during sample characterisations. I would like to acknowledge the grant received from University Research Grant 1001/PKIMIA/8011071 and 304/PKIMIA/6316598 Universiti Sains Malaysia which supported this work. I would also like to thank my PhD colleagues and lab fellows; Rania, Usman, Muhd Kabir, Sadiq Gumel, Abdullahi Birniwa, Abubakar Chadi, Fatimah, Usman Saidu, Benjamin, Najwa, Fatin, Izzana for their assistance.

Finally, I would like to convey my heartfelt appreciation to my respected parents (Late Sarkin Fulani Alh. Sa'ad Abdullahi and Hajiya Safiyah Muhammad Bello), My wife's mother Hajiya Amina Akilu and her family, and also my Respected Brothers

For their constant encouragement, support, and prayers, Alh. Nasiru, Zubairu, Musa, Sulaiman, Abdullahi and Sisters Haj Halima, Wakilatu, Maimuna and Ummal Kulsum. I will not forget my late brother Alh. Sulaiman Abdullahi and Sunusi Sa'ad, may ALLAH forgive and grant them Aljannatul Firdaus. My special thanks and appreciation go to my wife Fariliyya Yunusa Ibrahim and my children Safiyyah, Amina, Abdullahi and Fatimah, for their prayers, unconditional love, support, tireless sacrifice, and patience during this programme. May ALLAH reward you abundantly.

Finally, I am also grateful to Hussaini Adamu Federal Polytechnic, Kazaure, Nigeria for giving me ample opportunity to travel to Malaysia for my PhD programme. I also thank the Federal Ministry of Education and Tertiary Education Trust Fund (TETFund), Nigeria, for the award of PhD scholarship.

## TABLE OF CONTENTS

<b>ACKNOWLEDGEMENT.....</b>	<b>ii</b>
<b>TABLE OF CONTENTS .....</b>	<b>iv</b>
<b>LIST OF TABLES .....</b>	<b>x</b>
<b>LIST OF FIGURES .....</b>	<b>xii</b>
<b>LIST OF SYMBOLS .....</b>	<b>xv</b>
<b>LIST OF ABBREVIATIONS .....</b>	<b>xvi</b>
<b>ABSTRAK</b> ..... .....	<b>xix</b>
<b>ABSTRACT</b> ..... .....	<b>xxi</b>
<b>CHAPTER 1 INTRODUCTION .....</b>	<b>1</b>
1.1 Background .....	1
1.2 Problem Statements.....	4
1.3 Objectives.....	6
1.4 Scope of the Research .....	7
1.5 Thesis Layout .....	7
<b>CHAPTER 2 .....</b>	<b>LITERATURE</b>
<b>REVIEW .....</b>	<b>8</b>
2.1 General introduction.....	8
2.1.1 Epoxidized natural rubber .....	9
2.1.2 Liquid epoxidized natural rubber .....	11
2.2 Catalyst.....	16
2.2.1 Photocatalyst and concept of photocatalysis.....	17

2.2.2	Principles of heterogeneous catalysis.....	17
2.2.3	Photocatalyst band structure .....	19
2.3	Material for photocatalysis.....	20
2.3.1	Factors Affecting Photocatalytic Activity.....	22
2.3.1(a)	Light irradiation.....	23
2.3.1(b)	Concentration.....	24
2.3.1(c)	Band gap energy .....	25
2.3.1(d)	Crystallinity .....	27
2.3.1(e)	Surface area .....	28
2.3.1(f)	Pore volume.....	29
2.3.1(g)	Surface density .....	30
2.3.1(h)	Catalyst support .....	30
2.4	Modification of semiconductor photocatalyst.....	31
2.4.1	Doping of metals and non-metals .....	31
2.4.1(a)	Clay minerals overview .....	33
2.4.1(b)	Structure and properties of clay minerals .....	34
2.5	Polymer Degradation Using Metal Compounds as Catalyst.....	50
2.6	Metal-based supported catalysts .....	51
2.7	Methods of Introducing Metal Salts on HNT Supports .....	51
2.7.1	Deposition-Precipitation Technique.....	51
2.7.2	Precipitation/ Co-precipitation Method.....	52
2.7.3	Sol-gel Method.....	52
2.7.4	Impregnation Method.....	53
<b>CHAPTER 3</b>	<b>MATERIALS AND METHODS .....</b>	<b>56</b>
3.1	Experiment .....	56

3.1.1	Materials.....	57
3.2	Preparation of Metal-Based Supported HNT Catalysts .....	57
3.2.1	Synthesis of Ni <sup>2+</sup> -HNTs, and NiO-HNTs, calcined at 550 °C .....	57
3.2.2	Synthesis of calcined CuO-HNT <sub>N</sub> , NiO-HNT <sub>N</sub> , Co <sub>3</sub> O <sub>4</sub> -HNT <sub>N</sub> , CrO-HNT <sub>N</sub> , and ZnO-HNT <sub>N</sub> at 550 °C.....	57
3.2.3	Synthesis of various wt% of ZnO-HNT <sub>N</sub> calcined at 550 °C .....	58
3.2.4	Catalysts, LENR and degraded LENR denotations .....	59
3.3	Characterization of Catalysts .....	60
3.3.1	Fourier Transform Infrared Spectroscopy (FT-IR) .....	60
3.3.2	X-ray Diffraction (XRD).....	60
3.3.3	Field Emission Scanning Electron Microscope Coupled with Energy Dispersive X-ray Spectrometry (FESEM/EDX) analysis.....	61
3.3.4	Atomic Absorption Spectroscopy (AAS).....	61
3.3.5	Nitrogen adsorption-desorption .....	61
3.3.6	Optical Properties (UV-Visible Spectroscopy (UV-Vis) analysis.....	62
3.3.7	Photoluminescence (PL) analysis .....	62
3.4	Catalytic degradation of LENR.....	63
3.4.1	Degradation of LENR using Nickel sulphate based catalysts .....	63
3.4.2	Degradation of LENR using Various Metal Oxides-HNT catalysts (Nitrates based).....	63
3.4.3	Degradation of LENR using Various wt% of ZnO-HNT catalysts .....	63
3.5	Characterization of P-LENR and degraded LENR .....	64
3.5.1	Gel permeation chromatography (GPC). ....	64

3.5.2	Thermogravimetric Analysis (TGA).....	64
3.6	Reusability of the Photocatalysts .....	64
<b>CHAPTER 4 ..... FACILE SYNTHESIS AND PROPERTIES OF Ni-BASED SUPPORTED HOLLOYSITE NANOTUBE (HNT) CATALYSTS AND THEIR ROLE IN PHOTOCATALYTIC DEGRADATION OF LIQUID EXPOXIDIZED NATURAL RUBBER (LENR) ..... 65</b>		
4.0	Introduction .....	65
4.1	Characterization of HNT, un-calcined and calcined catalyst.....	65
4.1.1	FTIR Spectroscopy .....	65
4.1.2	X-Ray Diffraction (XRD) .....	67
4.1.3	Scanning Electron Microscopy Coupled with Energy Dispersive X-ray Spectroscopy (SEM/EDX).....	70
4.1.4	Atomic Absorption Spectroscopy .....	72
4.1.5	Nitrogen adsorption-desorption Analysis .....	72
4.1.6	Optical Study.....	74
4.2	Characterization of P-LENR and degraded LENR .....	76
4.2.1	Gel Permeation Chromatography (GPC) .....	76
4.2.2	FT-IR spectrum of P-LENR and degraded LENR.....	78
4.2.3	Thermogravimetric Analysis and Differential Thermograms .....	81
4.3	Comparative discussion of present work with previous literature .....	83
4.4	Summary .....	86
<b>CHAPTER 5 ..... COMPARATIVE STUDY OF THE PHOTOCATALYTIC DEGRADATION OF LENR BY VARIOUS METAL OXIDE-SUPPORTED HNT.....</b>		
		<b>87</b>
5.0	Introduction .....	87
5.1	Comparison of metal oxides supported HNT prepared from different metal salts.....	87



5.1.1	Gel permeation chromatography (GPC) .....	87
5.1.2	FT-IR of P-LENR and D-LENR .....	88
5.2	Comparison of various metal oxides supported HNT prepared from Nitrate salts.....	91
5.2.1	Characterization of CuO-HNT <sub>N</sub> , NiO-HNT <sub>N</sub> , Co <sub>3</sub> O <sub>4</sub> -HNT <sub>N</sub> , CrO-HNT <sub>N</sub> , and ZnO-HNT <sub>N</sub> .....	91
5.2.1(a)	Fourier Transform Infrared Spectroscopy (FTIR)	91
5.2.1(b)	X-ray Diffraction (XRD) .....	92
5.2.1(c)	Field Emission Scanning Electron Microscope Coupled with Energy Dispersive X-ray Spectrometry (FESEM/EDX) Analysis.....	95
5.2.1(d)	Atomic Absorption Spectroscopy.....	96
5.2.1(e)	Nitrogen adsorption-desorption Analysis .....	97
5.2.1(f)	Optical Study .....	100
5.3	Photodegradation of LENR by Various Metal-Oxide-HNT .....	102
5.3.1	Gel Permeation Chromatography (GPC) .....	102
5.3.2	FT-IR of P-LENR and degraded LENR.....	103
5.3.3	Thermogravimetric Analysis and Differential Thermograms .....	106
5.4	Higher photocatalytic efficiency of ZnO-HNT over other metal oxides .....	108
5.5	Comparative discussion of present work with previous literature .....	108
5.6	Summary .....	112
<b>CHAPTER 6 ... FACILE SYNTHESIS AND CHARACTERIZATION OF ZINC OXIDE (ZnO-HNT) PHOTOCATALYST SUPPORTED HALLOYSITE NANOTUBES FOR IMPROVED PHOTOCHATALYTIC DEGRADATION OF LIQUID EXPOXIZED NATURAL RUBBER .....</b>		<b>113</b>
6.0	Introduction .....	113
6.1	Characterization of 2, 4, 6 wt% ZnO-HNT <sub>N</sub> catalysts .....	113
6.1.1	FTIR of HNT and ZnO-HNT <sub>N</sub> Catalysts. ....	113

6.1.2	X-ray Diffraction (XRD).....	115
6.1.3	Field Emission Scanning Electron Microscope Coupled with Energy Dispersive X-ray Spectrometry (FESEM/EDX) analysis.....	117
6.1.4	Atomic Absorption Spectroscopy .....	119
6.1.5	Nitrogen adsorption-desorption Analysis .....	119
6.1.1	Optical Study.....	121
6.2	Photodegradation and Characterization of Degraded LENR .....	122
6.2.1	Effect of Different wt % of ZnO-HNT (2 wt%, 4wt%, and 6wt%) .....	122
6.2.2	Gel Permeation Chromatography (GPC) .....	122
6.2.2(a)	Thermogravimetric Analysis and Differential Thermograms.....	123
6.2.3	Effect of Photodegradation Time .....	126
6.2.3(a)	Gel Permeation Chromatography (GPC).....	126
6.2.3(b)	Thermogravimetric Analysis and Differential Thermograms.....	129
6.3	Reusability.....	132
6.3.1	Determination of possible photocatalyst supports (HNT) degradation.....	133
6.3.2	Summary .....	135

## CHAPTER 7

.....	137
-------	-----

7.1	Conclusions .....	137
7.2	Future recommendations .....	138

## REFERENCES

.....	139
-------	-----

## LIST OF PUBLICATIONS

## LIST OF TABLES

	<b>Page</b>
Table 2.1      Comparison of the degradation methods, conditions, and performance of catalysts on ENR/LENR	14
Table 2.2      Basic properties of HNT and CNT	36
Table 3.1      Catalysts formulation for various metal oxides -HNT <sub>N</sub> catalysts	58
Table 3.2      Catalysts formulation for ZnO-HNT with various wt %	58
Table 3.3      Pristine and degraded LENR denotation using various catalysts at different times	59
Table 4.1      The actual quantity of Ni in 4 wt% Ni-based-HNT photocatalysts obtained after AAS analysis	72
Table 4.2      Surface properties of various Ni-based HNT composite	74
Table 4.3      Weight average molecular weights (M <sub>w</sub> ), number average molecular weights (M <sub>n</sub> ) and polydispersity indexes (PDI) of P-LENR and degraded LENR	77
Table 4.4      Thermogravimetric analysis (TGA) results of P-LENR and degraded LENR	82
Table 4.5      Comparison of the degradation methods, conditions, and performance of catalysts on ENR/LENR	84
Table 5.1      Weight average molecular weights (M <sub>w</sub> ), number average molecular weights (M <sub>n</sub> ), and polydispersity indexes (PDI) of P-LENR and degraded LENR	88
Table 5.2      The actual quantity of different metals in 4 wt% metal oxides-HNT obtained after AAS analysis	97

Table 5.3	Comparison of surface properties of various Metal oxide-based HNT composites.....	99
Table 5.4	$M_w$ , $M_n$ and PDI of P-LENR and degraded LENR.....	103
Table 5.5	TGA results of P-LENR and degraded LENR.....	107
Table 5.6	Comparison of the degradation methods, conditions, and performance of catalysts on ENR/LENR.....	110
Table 6.1	Actual quantity of Zn in 2, 4 and 6 wt% ZnO-HNT obtained after AAS analysis.....	119
Table 6.2	Comparison of surface properties of various ZnO-based HNT composites.....	120
Table 6.3	$M_w$ , $M_n$ and PDI of P-LENR and degraded LENR .....	123
Table 6.4	TGA result of P-LENR and degraded LENR treated with (2, 4, and 6wt% ZnO-HNT <sub>N</sub> .....	126
Table 6.5	$M_w$ , $M_n$ , and PDI of P-LENR and degraded LENR at different time intervals (1, 2, 3, 5 and 7 Hours .....	128
Table 6.6	Thermogravimetric analysis (TGA) result of P-LENR and degraded LENR .....	131
Table 6.7	Weight of 4wt% ZnO-HNT <sub>N</sub> photocatalyst before and after several cycles of photocatalytic reactions .....	134

## LIST OF FIGURES

	<b>Page</b>
Figure 2.1    Structure of LENR.....	12
Figure 2.2    Factors affecting photocatalysts activity.....	23
Figure 2.3    Chemical structure of HNT.....	36
Figure 3.1    Experimental flow chat .....	56
Figure 4.1    FT-IR spectra of (a) HNT, (b) Ni <sup>2+</sup> -HNTs, (c) Calcine NiO-HNTs, at 550 °C .....	67
Figure 4.2    (a) HNT (b) Ni <sup>2+</sup> -HNTs (c) Calcined NiO-HNTs at 550 °C. ....	69
Figure 4.3    SEM image of (a) HNT, (b) Ni <sup>2+</sup> -HNTs, (c) calcined NiO-HNTs at 550 °C (d) average particle size of calcined NiO-HNTs.....	71
Figure 4.4    EDX image of uncalcined Ni <sup>2+</sup> -HNTs .....	71
Figure 4.5    Typical N <sub>2</sub> adsorption-desorption isotherms (BET) for (a) HNT (b) Ni <sup>2+</sup> -HNTs, (c) calcined NiO-HNTs at 550 [Inset: BJH pore size distribution plot].....	74
Figure 4.6    (a) UV-Vis absorption spectra (b) band gap energies (c) Photoluminescence of HNT, Ni <sup>2+</sup> -HNTs, Calcined NiO-HNTs at 550 °C .....	76
Figure 4.7    FT-IR spectrum of (a) P-LENR (b) 3H D-LENR (no catalyst) (c) 3H D-LENR (Ni <sup>2+</sup> -HNTs), (d) 3H D-LENR (NiO-HNTs), (e) 5H D-LENR (NiO-HNTs), (f) 7H D-LENR (NiO-HNTs).....	80
Figure 4.8    (a) TGA and (b) DTG thermograms of P-LENR and photodegraded LENR treated with and without catalysts. ....	82
Figure 5.1    FT-IR Spectra of (a) P-LENR b) 3H D-LENR (no catalyst) (c) 3H D-LENR (NiO-HNTs). (d) 3H D-LENR (NiO-HNT <sub>N</sub> ) .....	90

Figure 5.2	FT-IR spectra of (a) HNT (b) CuO-HNT <sub>N</sub> (c) NiO-HNT <sub>N</sub> (d) Co <sub>3</sub> O <sub>4</sub> -HNT <sub>N</sub> (e) CrO-HNT <sub>N</sub> (f) ZnO-HNT <sub>N</sub> calcinated at 550 °C.....	92
Figure 5.3	(a) HNT Calcined (b) CuO-HNT <sub>N</sub> (*), (c) NiO-HNT <sub>N</sub> (#), (d) Co <sub>3</sub> O <sub>4</sub> -HNT <sub>N</sub> (@), (e) CrO-HNT <sub>N</sub> (&) and (f) ZnO-HNT <sub>N</sub> (\$) at 550 °C catalysts.....	95
Figure 5.4	SEM image of (a) HNT, (b) CuO-HNT <sub>N</sub> , (c) NiO-HNT <sub>N</sub> , (d) Co <sub>3</sub> O <sub>4</sub> -HNT <sub>N</sub> , (e) CrO-HNT <sub>N</sub> , (f) ZnO-HNT <sub>N</sub> calcined at 550 °C.....	96
Figure 5.5	Typical N <sub>2</sub> adsorption-desorption isotherms (BET) for (a) HNT (b) CuO-HNT <sub>N</sub> (c) NiO-HNT <sub>N</sub> (d) Co <sub>3</sub> O <sub>4</sub> -HNT <sub>N</sub> (e) CrO-HNT <sub>N</sub> and(f) ZnO-HNT <sub>N</sub> calcine at 550 °C [Inset: BJH pore size distribution plot. ....	99
Figure 5.6	<b>(a)</b> UV-Vis absorption spectra <b>(b)</b> band gap energies <b>(c)</b> PL emission spectra with 1% attenuator of HNT, Calcined CuO-HNT <sub>N</sub> , NiO-HNT <sub>N</sub> , Co <sub>3</sub> O <sub>4</sub> -HNT <sub>N</sub> , CrO-HNT <sub>N</sub> and ZnOHNT <sub>N</sub> at 550 °C .....	102
Figure 5.7	FT-IR Spectra of (a) P-LENR, (b) 3H D-LENR (no catalyst), (c) 3H D-LENR (CuO-HNT <sub>N</sub> ), (d) 3H D-LENR (NiO-HNT <sub>N</sub> ), (e) 3H D-LENR (Co <sub>3</sub> O <sub>4</sub> -HNT <sub>N</sub> ), (f) 3H D-LENR (CrO-HNT <sub>N</sub> ), (g) 3H D-LENR (ZnO-HNT <sub>N</sub> ) .....	105
Figure 5.8	(a and b) showed TGA and DTG spectra of P-LENR, 3H D-LENR (no catalyst), 3H D-LENR (CuO-HNT <sub>N</sub> ), 3H D-LENR (NiO-HNT <sub>N</sub> ), 3H D-LENR (Co <sub>3</sub> O <sub>4</sub> -HNT <sub>N</sub> ), 3H D-LENR(CrO-HNT <sub>N</sub> ), and 3H D-LENR (ZnO-HNT <sub>N</sub> ). ....	107
Figure 6.1	FTIR spectra of (a) HNT (b) 2wt% ZnO-HNT <sub>N</sub> , (c) 4wt% ZnO-HNT <sub>N</sub> , and (d) 6wt% ZnO-HNT <sub>N</sub> calcine at 550 °C.....	115
Figure 6.2	XRD spectra of (a) HNT (b) 2wt% ZnO-HNT <sub>N</sub> , (c) 4wt% ZnO-HNT <sub>N</sub> , (d) 6wt% ZnO-HNT <sub>N</sub> , calcine at 550 °C. ....	117
Figure 6.3	SEM images of (a) HNT (b) 2wt% ZnO-HNT <sub>N</sub> , (c) 4wt% ZnO-HNT <sub>N</sub> , (d) 6wt% ZnO-HNT <sub>N</sub> calcine at 550 °C. ....	118

Figure 6.4	Typical N <sub>2</sub> adsorption-desorption isotherms (BET) for (a) HNT (b) 2wt% ZnO-HNT <sub>N</sub> (c) 4wt% ZnO-HNT <sub>N</sub> (d) 6wt% ZnO-HNT <sub>N</sub> calcines at 550 °C [Inset: BJH pore size distribution plot].....	120
Figure 6.5	(a) UV-Vis absorption spectra (b) band gap energies and (c) PL emission spectra with 1% attenuator of HNT, 2wt%, 4wt%, and 6wt% ZnO-HNT <sub>N</sub> calcined at 550 °C. ....	122
Figure 6.6	(a) showed TGA spectra of P-LENR and photodegraded LENR treated without and with 0.05g (2wt%, 4wt%, and 6wt% ZnO-HNT <sub>N</sub> ) (b) DTG of P-LENR and photodegraded LENR treated without and with 0.05g (2wt%, 4wt%, and 6wt% ZnO-HNT <sub>N</sub> ) .....	125
Figure 6.7	LENR Percentage degradation and change in Molecular weight at different time intervals.....	128
Figure 6.8	(a) showed TGA spectra of P-LENR and photodegraded LENR treated without and with 0.05g ZnO-HNT <sub>N</sub> (b) DTG of P-LENR and photodegraded LENR treated without and with 0.05g ZnO-HNT <sub>N</sub> . ....	131
Figure 6.9	Recycle experiment for photocatalytic degradation of LENR using 4wt% ZnO-HNT <sub>N</sub> photocatalyst. ....	133
Figure 6.10	FTIR spectra of the recycled 4wt% ZnO-HNT <sub>N</sub> sample after a 5-successive cycle .....	135

## LIST OF SYMBOLS

$\theta$	Bragg angle
$^{\circ}\text{C}$	Degree Celsius
D	d-spacing
$T_{\text{end}}$	End temperature
$\beta$	Full width at half-maximum (FWHM)
$T_{\text{g}}$	Glass transition temperature
$T_{\text{max}}$	Maximum temperature
Mn	Number average molecular mass
D	Particle size
$T_{\text{onset}}$	Onset temperature
$T_{\text{offset}}$	Offset temperature
%	Percentage
$h^{+}$	Photogenerated hole
K	Scherrer constant
h $\nu$	Ultraviolet radiation
$M_{\text{w}}$	Weight average molecular mass
$\lambda$	wavelength
$2\theta$	2 Theta



## LIST OF ABBREVIATIONS

a.u	Absorbance
AAS	Atomic Absorption Spectroscopy
ATR	Attenuated total reflectance
BET	Brunauer-Emmett-Teller
BJH	Barret-Joyner-Halenda
CB	Conduction band
CNT	Carbon Nanotube
DTG	Derivative Thermogravimetry
DSC	Differential scanning calorimetric
D-LENR	Degraded Liquid Epoxidized Natural Rubber
e.g	For example,
eV	Electron volt
EDX	Energy Dispersive X-ray
ENR	Epoxidized Natural Rubber
e <sup>-</sup>	Negatively charged Electron
FESEM	Field Emission Scanning Electron Microscopy
FT-IR	Fourier transform infrared
g	Gram
GPC	Gel Permeation Chromatography
H	Hour

HO·	Hydroxyl radical
HMW	High Molecular Weight
HNT	Halloysite Nanotube
i.e	For example
l	Liter
LENR	Liquid Epoxidized Natural Rubber
LMW	Low Molecular Weight
M	Molar
mol	mole
MMT	Montmorillonite
NAD	Nitrogen Adsorption-desorption Analysis
NPs	Nanoparticles
OH <sup>-</sup>	Hydroxide ion
O <sub>2</sub> <sup>-</sup>	Superoxides radical
P-	Pristine
PDI	Polydispersity Index
PL	Photoluminescence
QCE	Quantum confinement effect
s	Seconds
TGA	Thermogravimetric analysis
UV-Vis DRS	UV-Visible Diffuse reflectance spectroscopy
VB	Valence band
W	Watt

wt %	Weight percentage
XRD	X-ray diffraction

**SINTESIS DAN PENCIRIAN PELBAGAI NANOKOMPOSIT HALOSIT  
BERASASKAN LOGAM UNTUK FOTO-DEGRADASI CECAIR GETAH ASLI  
TEREPOKSIDA**

**ABSTRAK**

Dalam penyelidikan ini, pelbagai fotomangkin oksida logam (CuO, NiO, Co<sub>3</sub>O<sub>4</sub>, CrO dan ZnO) disokong HNT telah disintesis melalui impregnasi basah pelbagai garam logam (Cu(NO<sub>3</sub>)<sub>2</sub>·3H<sub>2</sub>O, NiSO<sub>4</sub>·6H<sub>2</sub>O, Ni(NO<sub>3</sub>)<sub>2</sub>·6H<sub>2</sub>O, Co(NO<sub>3</sub>)<sub>2</sub>·6H<sub>2</sub>O, Cr(NO<sub>3</sub>)<sub>3</sub>·9H<sub>2</sub>O, dan Zn(NO<sub>3</sub>)<sub>2</sub>·6H<sub>2</sub>O) pada HNT, diikuti dengan teknik pengkalsinan. HNT dan fotomangkin dicirikan menggunakan teknik FTIR, XRD, AAS, SEM/EDX, BET, UV-Vis (DRS), dan PL dan keputusan mengesahkan pembentukan fotomangkin (CuO, NiO, Co<sub>3</sub>O<sub>4</sub>, CrO dan ZnO) disokong HNT. Fotopemangkin kemudiannya digunakan untuk penguraian LENR dengan adanya penyinaran UV. Penguraian foto LENR kepada rantai yang lebih pendek menggunakan mangkin oksida logam yang disokong, merupakan kaedah alternatif yang cekap berbanding penggunaan bahan kimia. Ia penting untuk industri polimer kerana keupayaannya menghasilkan komponen berat molekul rendah yang boleh digunakan sebagai bahan mentah. Jika dibandingkan dengan LENR tulen, kumpulan berfungsi LENR terdegradasi menunjukkan beberapa perubahan. Analisis GPC mendedahkan bahawa M<sub>w</sub> LENR yang terdegradasi telah dikurangkan secara mendadak, membawa kepada kemungkinan pemotongan rantai yang lebih banyak. Oleh itu, boleh dipastikan bahawa degradasi fotomangkin LENR adalah berkesan dengan kehadiran fotomangkin. M<sub>w</sub> LENR berkurangan selepas pendedahan cahaya UV tetapi meningkat dengan pemangkin Ni<sup>2+</sup>-HNT. M<sub>w</sub> 3H D-LENR(NiO-HNTs) berkurangan dengan ketara daripada 25,732 untuk

LENR murni kepada 2.344 g/mol apabila NiO-HNT digunakan selama 3 jam degradasi. Walau bagaimanapun, masa degradasi yang lebih lama mengakibatkan pertautan silang, rantai pendek yang tidak stabil terbentuk. Ini konsisten dengan penemuan TGA dan DTG. Prestasi fotomangkin yang disintesis menggunakan sulfat dan garam logam berasaskan nitrat telah dinilai dan keputusan menunjukkan bahawa prestasi fotomangkin yang diperoleh daripada garam nitrat mempunyai keupayaan degradasi LENR yang lebih baik. Garam logam berasaskan nitrat didapati lebih baik dalam sintesis fotomangkin. Ini mungkin disebabkan oleh kesan toksik sulfat yang mungkin telah menyahaktifkan spesies aktif untuk degradasi LENR. Fotomangkin 4wt% ZnO-HNT mempamerkan prestasi pemangkin yang sangat baik berbanding dengan fotomangkin berasaskan oksida logam lain untuk degradasi LENR. Oleh itu, fotomangkin 2, 4 dan 6 wt% ZnO-HNT telah digunakan untuk degradasi LENR dan keputusan menunjukkan bahawa 4wt% ZnO-HNT mempunyai prestasi degradasi yang lebih tinggi. Prestasi yang lebih tinggi bagi 4 wt% ZnO-HNT melebihi 2 dan 6 wt% ZnO-HNT mungkin disebabkan oleh penyebaran tapak aktifnya yang lebih baik pada permukaan dan lumen HNT serta kurang aglomerasi seperti yang dapat dilihat pada imej SEM dan sifat optikal fotomangkin. Selain itu, apabila masa degradasi diubah antara 1 hingga 7 jam, masa yang dioptimumkan ialah 3 jam penyinaran. Ini mungkin disebabkan pertautan silang rantai yang lebih pendek yang terbentuk semasa masa degradasi yang lebih lama yang disokong oleh keputusan TGA dan DTG.

# **SYNTHESIS AND CHARACTERIZATIONS OF VARIOUS METAL-BASED HALLOYSITE NANOCOMPOSITES FOR THE PHOTO-DEGRADATION OF LIQUID EPOXIDIZED NATURAL RUBBER**

## **ABSTRACT**

In this research, various metal oxides (CuO, NiO, Co<sub>3</sub>O<sub>4</sub>, CrO and ZnO) based supported HNT photocatalysts were synthesized via wet impregnation of various metal salts (Cu(NO<sub>3</sub>)<sub>2</sub>·3H<sub>2</sub>O, NiSO<sub>4</sub>·6H<sub>2</sub>O, Ni(NO<sub>3</sub>)<sub>2</sub>·6H<sub>2</sub>O, Co(NO<sub>3</sub>)<sub>2</sub>·6H<sub>2</sub>O, Cr(NO<sub>3</sub>)<sub>3</sub>·9H<sub>2</sub>O, and Zn(NO<sub>3</sub>)<sub>2</sub>·6H<sub>2</sub>O) on HNT, followed by subsequent calcination techniques. HNT and photocatalysts were characterized by FTIR, XRD, AAS, SEM/EDX, BET, UV–Vis (DRS), and PL techniques and results confirmed the successful formation of photocatalysts (CuO, NiO, Co<sub>3</sub>O<sub>4</sub>, CrO and ZnO) supported HNT. The photocatalysts were subsequently employed to degrade LENR in the presence of UV irradiation. The photodegradation of LENR into shorter chains using metal oxide-supported catalysts is an alternative method which is efficient compared to the use of chemicals. It is significant for polymer industries due to its ability to produce low molecular weight components that can be used as raw materials. When compared to pristine LENR, the functional groups of degraded LENR exhibited some changes. GPC analysis reveals that the  $M_w$  of the degraded LENR was dramatically reduced, leading to the possibility of more chain scission. Thus, it can be established that the photocatalytic degradation of LENR is effective in the presence of photocatalysts. The  $M_w$  of LENR decreases after UV light exposure but increases with Ni<sup>2+</sup>-HNT catalyst. The  $M_w$  of 3H D-LENR(NiO-HNTs) reduced significantly from 25,732 for pristine LENR to 2,344 g/mol when calcined NiO-HNT was used for 3 hours of

degradation. However, longer degradation times resulted in the crosslinking of short unstable chains formed. This is consistent with the TGA and DTG findings. The performance of the photocatalysts synthesized using sulphates and nitrates-based metal salts was assessed and the results reveal that the performance of the photocatalysts derived from nitrates salts have better LENR degradation ability. Nitrates based metal salts was found to be better in the synthesis of photocatalyst. This may be due to the toxic effect of sulphates which may have deactivated the active species for degradation of LENR. 4 wt% ZnO-HNT photocatalyst exhibited excellent catalytic performance compared to other metal oxides based photocatalysts for the degradation of LENR. Hence, 2, 4 and 6 wt% ZnO-HNT photocatalysts were used for the LENR degradation and the results showed that 4wt% ZnO-HNT has higher degradation performance. The higher performance of 4 wt% ZnO-HNT over 2 and 6 wt% ZnO-HNT might be attributed to its better dispersion of active sites on the surface and lumen of HNT and less agglomeration as can be seen on SEM images and optical properties of the photocatalysts. Moreover, when degradation time was varied between 1 to 7 hours, the optimized time was 3 hours irradiation. This could be due the crosslinking of shorter chains formed during longer degradation times which was supported by TGA and DTG results.

# CHAPTER 1

## INTRODUCTION

### 1.1 Background

Polymers find application in several industries and can be sourced from both renewable and non-renewable sources. However disposing of them often, especially non-renewable ones, pollutes the environment (Tan & Abu Bakar, 2023). The benefits of depolymerizing polymers include the production of shorter-chained monomers with distinct qualities and high purity as well as the replacement of non-renewable resources (Tasakorn & Amatyakul, 2008)(Tan & Abu Bakar, 2023). Research on natural polymers and their degradation to improve their applicability in various fields has led to the development of shorter chain lengths with unique properties. For example, Liang et al. (2024) reported a green method for lignin depolymerization using  $\text{MoS}_2/\text{ZnO}$  heterojunction photocatalysts while Li and Zhang studied the chemical depolymerization and photoreforming of waste PET plastic, utilizing a binuclear zinc catalyst under mild conditions (Liang et al., 2024). Recently, photocatalytic depolymerization has gained considerable interest, due to its remarkable potential (Toor et al., 2011, Liu et al., 2019). Photocatalytic degradation is more effective when metal-based catalyst is used in the chemical reaction. It is regarded as effective due to the catalysts employed are non-toxic, simple to manufacture, and inexpensive, and sunlight might be use as a source of energy. Photocatalytic degradation derives the attention of many researchers in recent years due to the ability of visible light to initiate the process (Liu et al., 2019). Photocatalysis is an environmentally friendly approach that has arisen as a viable option for the degradation of a many of organic contaminants caused by fossil fuels, poor waste management, energy



crisis caused by the rapid technological advancement and population growth (Koe et al., 2019). Photocatalysts are derived mostly from metal-based substances usually metal oxides and hydroxides referred to as semiconductors.

Metal oxides nanoparticles have become more relevant in recent years in a variety of sectors, including physics, medicinal research, chemistry, and material science (Karthikeyan et al., 2020). Metal-based compounds have good catalytic performance for polymer degradation, but their high tendency to agglomerate together into bigger particles makes recovery and separation difficult, which lowers their effectiveness (Tan & Abu Bakar, 2023). It has been established in the literature that when some metal atoms are not in contact with the reactant particles, they are considered waste (Liu, 2017); however, to overcome these challenges during photocatalysis, the metal-based nanoparticles must be synthesized and disperse evenly on the surface of highly eco-friendly support with a higher surface area to volume ratio and scientist observed that the use of clay minerals as the best solution.

Clay minerals are very attractive materials used as catalyst supports in recent years due to their outstanding properties, like high thermal stability, resistance to chemical attack, everlasting micro/mesoporosity structure, low toxicity, high surface area, and pore volume (Son et al., 2021). The dispersion of catalytic active sites on the clay surface stops semiconductor agglomerations, lowers optical bandgap reduces electron-holes recombination increases contact between reactant particles and catalyst (Marković et al., 2018). Among the eco-friendly clay minerals, Halloysite nanotube (HNT), plays an important role in several aspects including catalytic support due to its unique characteristics.

HNT is dioctahedral 1:1 clay mineral present in weathered rocks and wet tropical and subtropical areas (Madureira & Bastien, 2021). It is mostly found in abundance in countries like New Zealand, China, Belgium, and France (Madureira & Bastien, 2021). However, the presence of O-H group on the HNT surface and lumen provides a better opportunity of its modification and dispersion properties which results in the improving its properties. HNT has been modified by many researchers for making catalysts material using metal ions, metal hydroxides, dendrimers, metal oxides, and chitosan, which are used for special applications such as adsorption (Zango et al., 2017, Nyankson et al., 2019), photocatalytic degradation of organic contaminants (Peng et al., 2017). Research has shown the modification of HNT with metal-based semiconductors as catalysts improved their photocatalytic performance. Peng et al. studied the synthesis of ZnO/HNT catalysts and its photocatalytic activity on methylene blue dyes (MB) was evaluated in the presence of UV-irradiation and the results show excellent degradation of MB (Peng et al., 2017). Mishra and Mukhopadhyay reported the TiO<sub>2</sub> decorated functionalized HNT, (TiO<sub>2</sub>/HNT) nanoparticle photocatalyst preparations used for the degradation methylene blue (MB) and rhodamine B (RB) in wastewater treatment, the result demonstrates their excellent degradation ability (Mishra & Mukhopadhyay, 2019). In another study, Wang et al. prepared Pt@ RHNT catalysts photocatalyst by loading Pt on HNT, which demonstrates speedy rates of hydrogenation reactions with outstanding resistance to leaching after being used and reused, moreover, titanium and platinum-based catalyst are very expensive, therefore low-cost metals or metal oxide semiconductors need to be used with HNT support for the preparation of efficient photocatalysts.

## 1.2 Problem Statements

In the recent decade, various techniques were used for the depolymerization (degradation) of biopolymers to obtain fine chemicals which are used for the preparation of primary industrial raw materials to substitute petroleum-based chemicals due to deflation of the resources and global warming caused by the burning of fossils fuel i.e., Mechanical (milling), chemical, oxidative, thermal, and photocatalytic degradation have been used for the degradation of ENR/ LENR. All these methods achieve some degree of degradation, however, at times, hazardous chemical additives and long reaction times are required. For instance, oxidative degradation of ENR/LENR occurred in the presence of a catalyst between 0.5-10 g, required heat, and for a duration of 10-20 hours to obtain 53-95 % degradation efficiency. While chemical degradation methods take place between 8-30 hours, using a 6-20 g catalyst, in the presence of heat and yielded 67-98 % degradation. In contrast the thermal degradation method reported the use of 0.5-250 g catalyst for 4-6 reaction time in the presence of heat, which produced 65-89 % degradation (Talib et al., 2019) (Basheer et al., 2020)(Salehuddin et al., 2018). LENR degradation was firstly reported by Talib et al., (2019). In their work, only 9.25 wt%  $\text{La}(\text{OH})_3\text{-HNT}$  was investigated. Other wt % of catalysts were not investigated. Furthermore, the time taken to do the degradation was 6 hours and the percentage of the degradation was reported to be 88%. Talib's work demonstrated the feasibility of LENR degradation using the thermal method with  $\text{La}(\text{OH})_3\text{-HNT}$  catalyst. However, there still exists research gaps. First, cheaper metal oxide/HNT catalyst can be considered. Furthermore, a systematic approach to determine the ideal loading of metal oxide on HNT for degradation of LENR can be conducted. The recyclability of the photocatalyst is another aspect that can be studied.

Subsequently, the photocatalytic method can be considered as a more energy efficient technique for the degradation of LENR. However, not many studies using photocatalytic depolymerization has been carried out.  $\text{TiO}_2/\text{H}_2\text{O}_2$  was recently used to convert ENR to LENR but 232 g of the photocatalysts were used in 24 hours to achieve 90 % degradation (Ibrahim et al., 2022). The main drawback of their work was the use of  $\text{H}_2\text{O}_2$  as initiator, which is not able to be recovered for reusability and the degradation is more effective at higher reaction times of 48 hours. To overcome this, an important factor to consider when synthesizing catalysts is to use a support which can prevent agglomeration of the active phase as well as be advantages for easy recovery. The tubular structure of HNTs offers large surface area and stability, making them suitable natural supports for metal oxide catalysts. Previous work have demonstrated that HNTs have been loaded with metal oxides such as CuO and  $\text{Co}_3\text{O}_4$  to improve their photocatalytic capabilities, have synergistic effects and long-term stability (Carrillo & Carriazo, 2015).

To date, few studies have been conducted on the photocatalytic degradation of biopolymers using metal oxide-based supported catalysts, such photocatalysts offer several advantages, including simplicity, low cost, environmental-friendly and low energy consumption. However, no reports have been made on the application of these photocatalysts for the photocatalytic degradation of LENR. Therefore, in this research work various metal oxides supported HNT photocatalysts are synthesized and their roles in the photocatalytic degradation of LENR without the use of expensive and carcinogenic initiators and at the shortest possible degradation time are scientifically studied.

### 1.3 Objectives

The research objectives are as follows:

1. To synthesize and understand the properties of  $\text{Ni}^{2+}$ -HNT as well as NiO-HNT for the photodegradation of LENR at different times.
2. To compare the effect of different metal salts as well as various metal oxides (CuO, NiO,  $\text{Co}_3\text{O}_4$ , CrO and ZnO) supported HNT for the photodegradation of LENR characterized by GPC technique.
3. To investigate the effect of parameters such as weight % of ZnO supported on HNT, catalyst loading and degradation time towards the photodegradation of LENR in terms of degree of degradation.

## **1.4 Scope of the Research**

This work will only be focused on the preparation of Ni metal salts and several metal oxides (CuO, NiO, Co<sub>3</sub>O<sub>4</sub>, CrO and ZnO) supported by HNT as catalysts for the photocatalytic degradation of LENR. The photocatalysts will be synthesized by the impregnation method. The HNT, Ni metal salt supported HNT and metal oxide supported HNT catalysts will be characterized via XRD, FTIR, AAS, SEM, BET, UV-Vis (DRS), and PL analysis to understand the characteristics of the catalysts. The catalyst are then applied for the photodegradation of LENR with the aid of UV-irradiation technique. The pristine LENR and degraded LENR are analyzed using GPC, TGA and FTIR analysis.

## **1.5 Thesis Layout**

This thesis comprises of seven Chapters. The first Chapter contains an introduction, problem statements, objectives, and scope of the research work. Chapter two consists of a literature review, which covers recent findings on various techniques used for the depolymerization of LENR. Chapter three, described the materials, experimental procedures and characterization techniques used in this study. Chapter four, discussed the finding and observations of photocatalytic degradation of LENR using both uncalcined and calcined NiO-HNTs. Chapter five describes the comparative study on the synthesis, characterizations, and photocatalytic degradation of LENR using CuO-HNT<sub>N</sub>, NiO-HNT<sub>N</sub>, CoO-HNT<sub>N</sub>, CrO-HNT<sub>N</sub> and ZnO-HNT<sub>N</sub> photocatalysts. Chapter six discusses the comparative study on the synthesis, characterizations, and photocatalytic degradation of LENR using 2, 4 and 6 wt% ZnO-HNT and using the best photocatalyst and optimization of the reaction conditions. Chapter seven shows the conclusion and recommendations for future work in this area of research.

## CHAPTER 2

### LITERATURE REVIEW

#### 2.1 General introduction

Scientists are working to identify alternatives to fossil fuels in response to the rapid increase in industrial chemical needs, energy production as well as global warming brought on by population growth and industrialisation (Sabeeh et al., 2020). Research scientists are particularly interested in the degradation of polymeric materials because it frequently results in the production of novel materials that are either difficult to prepare or expensive to prepare using traditional polymerization methods (Salehuddin et al., 2020). Biopolymers degradation derived from forestry waste is currently one of the most promising alternate methods for producing energy and precious fine chemicals utilised as fundamental industrial raw materials (Liu et al., 2019).

Natural polymers, such as starch, lignin, pectin, cellulose, and chitin, are naturally found as biopolymers of plant and animal origin (Tan et al., 2022). However, synthetic polymers are long-chain polymers typically derived from petroleum-based primary raw materials (Tan et al., 2015). Synthetic polymers are more frequently employed in numerous applications than natural polymers due to their less expensive and more durable (Tan et al., 2022). However, in recent years they have caused tremendous pollution and global warming due to improper disposal and resistance to degradation when discarded into the environment (Bellah et al., 2012). As a result, research into using natural polymers as an alternative to produce fuel and fine chemicals has recently increased to generate green energy (Tan et al., 2016). Many researchers reported the degradation of polymers to produce molecules with shorter chain lengths with various unique features, which will help to increase the application of natural polymers in diverse industries (Tan et al., 2022). Biopolymer degradation resulted in the production of novel materials that are either

difficult to prepare or expensive to prepare through traditional chemical reactions (Salehuddin et al., 2020). These techniques are also utilized to enhance specific commercial polymer characteristics or to add reactive functional group intermediates to the polymer chains for further modification. In previous studies, several attempts have been made for the depolymerization of biopolymers via some methods, which include liquefaction (Toor et al., 2011, Zhu et al., 2015), hydrothermal carbonization (Kambo et al., 2018), oxidative, mechanical, gasification (Wang et al., 2021), pyrolysis (Li et al., 2015), hydrogenolysis (Li et al., 2015), catalytic oxidation (Liu et al., 2019), thermal degradation (Talib et al., 2019), and photodegradation (Ravindran et al., 1988)(Liu et al., 2019). it has been established that the major limitations of these methods are sided reactions, excess solvent use, high pressure, and temperature (Chio et al., 2019, Ma et al., 2019). Various methods were utilized for the biopolymers degradation, however, photocatalytic method gives outstanding efficiency (Toor et al., 2011), (Liu et al., 2019), (Ibrahim et al., 2020). Among the biopolymers, natural rubber is abundant with a variety of applications in the automobile and many industries (Salehuddin et al., 2018), (Yusof et al., 2021).

### **2.1.1 Epoxidized natural rubber**

ENR is a non-fossil fuel-based elastomer made by chemical modification of natural rubber through an epoxidation process in which an epoxy group is added into the NR polymer backbone to enhance the polarity of groups throughout the polymer chains while retaining the majority of the properties of its native counterpart (Arrigo et al., 2020). The presence of the epoxy group significantly enhances some of its properties (Jorge et al., 2010) compatibilizer (Harun & Chan, 2016), polarity, conductivity (Klinklai et al., 2006), Automotives (Ravanbakhsh et al., 2016), abrasion resistance, higher resilience, wet grip (Hong et al., 2005), adhesions and sealants (Poh & Soo, 2016)(Johnson & Thomas, 2000), clamps (Saito et al., 2007), reduced air permeability, better-



rolling resistance, improved oil, and solvent resistance (Tanrattanakul et al., 2003), adhesion (Poh & Gan, 2010), and thermal stability (Ibrahim et al., 2022). wire and cable (Harun & Chan, 2016), butyl and acrylonitrile rubber substitutes (Yang et al., 2010), and plastic toughening agents (Pichaiyut et al., 2016) are a few examples of the uses for this compound. ENR has recently been highlighted as materials for autonomous healing (Rahman et al., 2012)(Lin et al., 2014) and electronic applications (Lin et al., 2014)(Tan et al., 2013)(Mohammad et al., 2013).

It is formed via the introduction of epoxy linkage on the NR. ENR comprises shorter polymeric chains than conventional natural rubber, with part of the C=C being changed into the epoxy group (Azhar et al., 2015). Adding epoxide groups to the polymer chain can improve NR qualities, such as damping, oil resistance, wet grip, and gas permeability. Furthermore, the existence of epoxy groups scattered randomly in the polymer chains increases the compatibility of modified NR-containing polar groups. It makes filler distribution easier in the absence of coupling agents (Xu et al., 2015). As a result, ENR is being studied as a possible alternative to various synthetic elastomers (T. Xu et al., 2015). In the 1980s ENR became a commercial product. Peroxyl acids such as peracetic and per benzoic acid might easily epoxidize NR in solution. ENR is a derivative of NR and derived from an epoxidation process using latex or organic solutions (Azhar et al., 2017).

Two major reagents are employed in the industrial epoxidation process: peroxyacetic acid or a combination of formic acid and hydrogen peroxide. The epoxidation reaction can be carried out indefinitely to get any desired epoxy content. Only m-chloro perbenzoic acid can react quantitatively with the double bond among several organic peroxy acids. The epoxidation process has a 56.2 kJ/mol activation energy. The epoxidation yield is proportional to the reaction time of NR and peroxy acid concentrations (Vernekar et al., 1992). Numerous side reactions occur during

epoxidation, introducing functional groups, including tetrahydrofuran, hydroxyl, and ester, into the NR chain. Linear improvement of glass transition temperature ( $T_g$ ) occurred with an increase in the amount of epoxy by 1 mol %, as the epoxy content increased also  $T_g$  increased by around 1° C. The  $T_g$  of ENR with 25 mol % epoxidation (ENR25) is 47 °C, whereas the  $T_g$  of ENR with 50 mol% epoxidations (ENR50) at 22 °C. Many features of ENR are projected to improve as  $T_g$  increases, including better and stronger binding to metal, wet grip, fatigue behaviour, and tensile strength. When it comes to tire safety, a wet grip is a vital factor to consider. When braking on a wet road, tires with superior wet grip have a shorter distance to stop. The mechanical performance of NR changes dramatically as it crystallizes. As the degree of crystallization increases, there is a nonlinear increase in density and Young's modulus. ENR25 and ENR50 do not crystallize at low temperatures (Fuller et al., 2004). ENR is now used as the primary raw material to produce low molecular weight compounds used for several industrial applications. One of the derivatives of ENR is liquid epoxidized natural rubber (LENR).

### **2.1.2 Liquid epoxidized natural rubber**

LENR is a low  $M_w$  derivative of ENR with a shorter polymeric chain; compared to ENR, which is hard and rubber elastic, LENR has a soft and sticky appearance. It has been reported that LENR is prepared using chemicals on ENR through photocatalytic degradation, mechanical grading, ozonolysis, and thermal oxidation methods (Yusof et al., 2021). LENR has recently become an important starting material for the production of different industrial chemicals because of its efficiency of the reaction in liquid form, and the reactants can be mixed easily with lower energy usage (Yusof et al., 2018). Therefore, the degradation of LENR may lead to the formation of  $LM_w$  compounds with many applications in the industry, such as ketone, aldehydes, ethers, and alcohols, and can be a substitute for petroleum-based raw materials. Yusof et al. describe LENR

synthesis through ENR latex degradation using  $\text{NaNO}_2/\text{H}_2\text{O}_2$ . The latex conditions were adequate for preparing LENR, with a pH of 8.0 and a surfactant content of 2-3 w/w%. The  $M_n$  and  $M_w$  of ENR reduced drastically as the concentration of reagents increased, leading to the formation of LENR (Yusof et al., 2018). Figure 2.1 shows a typical LENR structure.

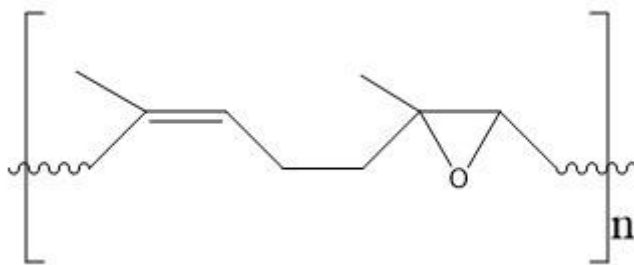


Figure 2.1 Structure of LENR

LENR is the derivative of ENR, which is obtained from the degradation of ENR, typically through mechanical grinding, chemical degradation in the presence of  $\text{K}_2\text{S}_2\text{O}_8$ , and photooxidation initiated by UV-irradiation (Rooshenass et al., 2016). ENR exhibits a typical chain cleavage that resembles that of NR, where the chain is oxidized and cleaved. Depending on the technique, the bond cleavage in ENR might happen in both the oxirane and double bond groups leading to the formation of LENR (Ibrahim et al., 2022). In another study, the UV degradation method resulted in a higher LENR yield within a shorter reaction time when compared with mechanical grinding and chemical degradation methods. The amount of ENR  $M_w$  degradation recorded within 4 hours of reaction time using the UV-photodegradation method was found to be more than the one obtained using both mechanical grinding (after 8 hours) and chemical degradation methods (after 15 hours) (Rooshenass et al., 2016). The preparation of LENR via UV irradiation is less costly. It produces very good chemical intermediates such as hydrofuran in addition to ketones, aldehydes, carboxylic acid, ester, and lactone, which are used in industry (Rooshenass et al., 2016).

Rooshenass et al. reported preparing LENR by oxidative degradations using periodic acid,  $\text{KMnO}_4$ , and UV irradiation (Rooshenass et al., 2017). They studied ENR oxidative degradation using periodic acid,  $\text{KMnO}_4$ , and UV irradiation. All three methods show a certain degree of degradation, but periodic acid was found to have the lowest Mn and fastest degradation rate. Each technique of ENR degradation has its own set of benefits and limitations, resulting in various functional groups with various mechanisms (Darji et al., 2021). The chemical reaction approach, such as sodium nitrite, phenyl hydrazine oxygen, and photocatalytic degradation, has received the attention of researchers due to allowing for greater control of the  $M_w$  product than the thermal and mechanical techniques. Besides being renewable, LENR degradation at the latex stage has a low viscosity, making it easier to process (Darji et al., 2021). Recently, reported the preparation of LENR via Photocatalytic degradation of ENR latex using hydrogen peroxide and  $\text{TiO}_2$  nanocrystals as photocatalysts. In this study, low  $M_w$  ENR50 was produced by degrading 50% mol of ENR50 under UV light in the latex state (LENR). In the presence of  $\text{TiO}_2$  as a photocatalyst and  $\text{H}_2\text{O}_2$  as a reagent, ENR50 latex was exposed to UV light. The GPC results demonstrated ENR50 latex degraded when subjected to UV irradiation.

Moreover, the ENR degradation increases in the presence of  $\text{H}_2\text{O}_2$  and  $\text{TiO}_2$ , and the molecular weight decreases drastically from  $161.77 \times 10^3$  g/mol to  $14.57 \times 10^3$  and  $6.40 \times 10^3$  g/mol after 24 and 48 h of irradiation, respectively. The presence of  $\text{TiO}_2$  did not affect the effectiveness of the degradation but caused the epoxy ring opening. The existence of carbonyl and hydroxyl groups in the degraded sample, which were caused by the chain breaking and ring opening, was confirmed by FTIR and NMR spectroscopic analysis (Ibrahim et al., 2022).

Table 2.1 Comparison of the degradation methods, conditions, and performance of catalysts on ENR/LENR  
Comparison of the degradation methods, conditions, and performance of catalysts on ENR/LENR

Catalyst	Method of degradation	Amount of catalyst used (g)	Temperature (°C)	Light Source	Degradation time (h)	Mw of ENR/LENR before/after degradation ( $M_w$ ) ( $\times 10^3$ ) g/mol	Percentage degradation (%)	Conversion	Ref.
La(OH) <sub>3</sub> -HNT	Thermal (Furnace)	0.5	250	-	6	18.984 – 2.111	89	LENR – degraded LENR	(Talib et al., 2019)
TiO <sub>2</sub> /H <sub>2</sub> O <sub>2</sub>	Photocatalytic	-	-	UV	24	161.77 - 14.57	90	ENR - LENR	(Ibrahim et al., 2022).
					48	161.77 - 6.400	96		
NaNO <sub>2</sub> /H <sub>2</sub> O <sub>2</sub>	Photocatalytic	16	-	UV	48	170.31- 56.19	67	ENR - LENR	(Yusof et al., 2021)
Sodium dodecyl sulfate/NaNO <sub>2</sub> / H <sub>2</sub> O <sub>2</sub>	Chemical	20	65-70	heat	8	299.50- 33.52	88	ENR - LENR	(Yusof et al., 2018)
H <sub>5</sub> IO <sub>6</sub>	Oxidative Degradation	-	30	-	10	695.000 - 31.400	95	ENR - LENR	(Rooshenas et al., 2017)
KMnO <sub>4</sub>	Oxidative	10	-	-	10	696.000- 205.000	71	ENR - LENR	(Rooshenas et al., 2017)
-	Photo	-	30	UV	18	696.000 – 16.800	97	ENR - LENR	(Rooshenas et al., 2017)
K <sub>2</sub> S <sub>2</sub> O <sub>8</sub>	Chemical Oxidation	6.4	60	-	30	695.508 – 10.476	98	ENR - LENR	(Rooshenas et al., 2016)

Table 2. 1 (continue)

Catalyst	Method of degradation	Amount of catalyst used (g)	Temperature (°C)	Light Source	Degradation time (h)	Mw of ENR/LENR before/after degradation ( $M_w$ ) ( $\times 10^3$ ) g/mol	Percentage degradation (%)	Conversion	Ref.
-	Milling	-	-	-	8	695.508 – 40.762	94	ENR - LENR	(Rooshenas et al., 2016)
-	Photo	-	50	UV	15	695.508 – 16.953	97	ENR - LENR	(Rooshenas et al., 2016)
H <sub>2</sub> O <sub>2</sub> /NaNO <sub>2</sub>	Redox reaction	-	70	-	8	254.380 – 45.340	82	ENR - LENR	(Yusof et al., 2018)

## 2.2 Catalyst

Catalysis has played a significant role in chemical research since its introduction in the chemical industry by J. Roebuck in 1746; approximately 85–90% of the chemical industries' products are now produced using catalytic processes (Massaro et al., 2020)(Massaro et al., 2017). According to basic knowledge of catalysis, the reaction is classified into two homogeneous and heterogeneous catalysis. Homogeneous catalysis is a chemical reaction in which both reactants, products, and catalysts are in the same phase. In contrast, heterogeneous catalysis is a chemical reaction in which the reactants, catalysts, and products are in different stages. The development of heterogeneous catalysts based on metal nanoparticles is receiving a lot of interest due to the restrictions of homogeneous catalysts (Massaro et al., 2020)(Massaro et al., 2017). The catalyst that exhibits nanoparticle properties has demonstrated a higher catalytic activity which makes them have exceptional applications because of their higher surface area and small size compared to conventional catalysts (Tharmavaram et al., 2018). The nanomaterials' structural dimensions (1–100 nm) allow them to acquire unique and improved properties such as magnetic, electrical, optical, and mechanical, and combined with significantly improved adsorption and catalytic properties to the bulk counterparts (Tharmavaram et al., 2018). The benefits of utilising catalysts made of metal-based nanoparticles in the chemical industry are related to pore size and particle characteristics being changed to improve catalytic selectivity and activity (Massaro et al., 2017). A catalytic reaction in which the catalyst is in a different phase with the reactants is known as heterogeneous photocatalysis. Five separate stages must occur for each heterogeneous reaction to occur: (i) reaction on the catalyst surface and production of new products, (ii) adsorption of specific reactants on the catalyst surface, (iii) reaction on the catalyst surface and synthesis of new products, (iv) desorption of products, and (v) diffusion of products into the fluid system (Zhang et al., 2012).

However, many techniques are used in industry and laboratories for applying catalysts during chemical reactions. Photocatalysis is one of the most effective techniques in recent decades.

### **2.2.1 Photocatalyst and concept of photocatalysis**

Photocatalysts are materials that can absorb light energy and use it to speed up photoreaction without being consumed. Photocatalysis is the process that takes place when a light source interferes with the photocatalyst's surface. It is a primary mechanism that involves two simultaneous reactions (oxidation and reduction reactions) of photogenerated holes and electrons, respectively. These charge-carrier combinations create a powerful oxidizing agent that degrades organic materials into CO<sub>2</sub> and H<sub>2</sub>O. Several light sources can be used for photocatalyst activation, including UV, visible, artificial, and sunlight (Abdullah et al., 2022)(Lee & Li, 2021).

### **2.2.2 Principles of heterogeneous catalysis**

Heterogeneous photocatalysis is essentially the term used to describe chemical processes that are catalyzed by the presence of light energy. When it comes to semiconductors are involved in heterogeneous photocatalysis, the catalysts needed for this process correspond to semiconductors that are responsive to light irradiation. The combination of photochemistry and catalysis is referred to as photocatalysis. The word "photocatalysis" comprises two components, photo and catalysis. Photo refers to light, while catalysis means changes in the rate of chemical reactions that occur because of the presence of a catalyst. Throughout any chemical reaction, catalysts do not undergo any permanent changes or participate as reactant constituents in product formation (Son et al., 2021). However, photocatalysis is described as accelerating a light-induced reaction derived electron in the presence of a catalyst. Both light and catalysts are used to accelerate a chemical process simultaneously. The light source (photon energy) and catalyst



(semiconductor) are the two most important components in the photocatalysis process (Son et al., 2021). Heterogeneous photocatalysis uses inorganic semiconductor photocatalysts such as  $\text{TiO}_2$ ,  $\text{CdS}$ ,  $\text{SnO}_2$ ,  $\text{ZnO}$ ,  $\text{CuO}$ ,  $\text{MoS}_2$ ,  $\text{Bi}_2\text{O}_3$ ,  $\text{ZrO}_2$ , and  $\text{WO}_3$ , which may produce electron/hole pairs when exposed to light ( $h\nu$ ) with an energy equal to or more than the semiconductor's bandgap energy (Li & Hu, 2016).

Photocatalytic efficiency is mostly determined by the photocatalyst's capacity to generate holes and long-lived electrons because of the formation of reactive-free radicals. The band gap, the distance between the valence (VB) and conduction bands (CB), is the least energy necessary to excite an electron to reach the CB. Band gaps exist in insulators, semiconductors, and conductors in different ways (Abdellah et al., 2018). The energy gap between the VB and the CB in insulators is rather significant. As a result, the electron jumps from VB to CB are limited. The VB overlaps the CB in a conductor, allowing valence electrons to migrate freely into the CB. The band gap in semiconductors is adequately small, and the electron excitation is usually initiated by solar radiation.

Without recombination, certain electrons and holes can migrate to the surface of a semiconductor and start redox reactions with the water and oxygen absorbed on the photocatalyst surface, which leads to the breakdown and mineralization of organic molecules. The heterogeneous photocatalytic process is widely known to consist of four stages, which comprise (i) light-harvesting (ii) photogeneration of charges (iii) charge transfer and recombination, and (iv) oxidation-reduction reactions. It is essential to understand that a reduce in the fractional performance at any stage can reduce the photocatalytic process's overall effectiveness (Li & Hu, 2016). When the surface of the photocatalyst is flat and smooth, an increased light reflection is predicted, which is bad for light harvesting and organic substance absorption (Li & Shi, 2016).

Highly uneven and porous photocatalysts allow various reflections and dispersion of light within the interiors of cavities and their pore channels, resulting in improved light consumption and the generation of more photoexcited  $e^-/h^+$  pairs to improve photocatalytic efficiency. Another key factor hindering the improvement of the photocatalytic process is the fast recombination of photoexcited electron-hole ( $e^-/h^+$ ) pairs on the photocatalyst surface. The charge carrier recombination rate is one of heterogeneous photocatalysis's most important and difficult aspects. Finally, considerable aggregation of nanostructured particles results in a low specific surface area, which decreases the rate of reduction and oxidation (Lee & Li, 2021). It further increases the diffusion boundaries of reagents. All these issues work against improving the photocatalytic process. In the case of photodegradation of organic substances in aqueous solutions, however, the increased rate of adsorption and diffusion of reactants in porous photocatalysts may meaningfully improve the effectiveness of the photocatalyst because of reduced mass transport boundaries and a faster rate of activation of the adsorbed species. The criteria described above have been shown to substantially impact the overall performance of photocatalysts in the heterogeneous photocatalytic process. These parameters must be addressed when used in practice to improve the effectiveness of the photocatalytic process (Li & Shi, 2016).

### **2.2.3 Photocatalyst band structure**

Any photo-based application relies on the capacity to photoexcite electrons in any crystalline semiconductor utilizing an external energy source. The energy bands, a collection of distinct energy levels of electrons around each atom, are populated by these electrons. Electrons in an isolated atom have only discrete energy levels. Due to atomic interactions, these energy levels are divided into multiple divisions in a crystalline solid, resulting in a continuous band of permissible energy states, like the VB and CB. The VB, which are made up of occupied molecular

orbitals with a lower energy level than the CB, are built-up occupied molecular orbitals. The CB is frequently empty, and its energy levels are higher. The band gap is the distance between the valence and CB in a semiconductor, and this is where the fermi level is found (50 % probability of occupied states)

### **2.3 Material for photocatalysis**

It has been established that photocatalysts made of metal oxide semiconductors are commonly good photocatalysts (Abdullah et al., 2022). Metal oxides are the most promising and commonly utilized semiconductor photocatalysts; examples of widely used semiconductors are CuO, Fe<sub>2</sub>O<sub>3</sub>, Bi<sub>2</sub>WO<sub>6</sub>, V<sub>2</sub>O<sub>5</sub>, TiO<sub>2</sub>, SnO<sub>2</sub>, ZnO, ZnS, WO<sub>3</sub>, MoO<sub>3</sub>, CeO<sub>2</sub>, ZrO<sub>2</sub>, NiO, NiO<sub>2</sub>, and CdS. Metal oxide-based semiconductor photocatalysts are preferred because of their unique properties and several advantages. The properties are adjustable size, solid oxidizing power, a large surface area/ pore volume, wide absorption ranges with high absorption coefficients, and a suitable optical band gap (Karthikeyan et al., 2020). They allow repeated electron transfer processes with the extended application without considerable loss of photocatalytic activity, being stable, cost-effective, environmentally friendly, and operating at ambient temperature and pressure (Duan et al., 2016). These photocatalysts are generally used due to their exceptionally narrow band gaps and electronic structure (occupied VB and unoccupied CB). The excitation of electrons, e<sup>-</sup>, from the VB to the CB with concurrent production of holes, h<sup>+</sup>, in the VB is what activates a semiconductor photocatalyst. This is done by its interaction with light of sufficient energy to start photocatalytic reactions. The photogenerated electron-hole pairs undergo recombination or various interfacial processes in which they interact with electron donors or acceptors. These mechanisms must successfully compete to enable the creation of reactive oxidising species.

The separation and transfer of photoelectrons and holes under irradiation, as well as the interaction between the active component and the reactants, are two major components of photocatalysis (Zou et al., 2022). The most important aspect of photocatalysis is allowing the active component to participate as much as possible in the photochemical process while maintaining maximum exposure to active sites and adsorption reactants (Zou et al., 2022).

Metal-based catalysts play an important role in several industrial and laboratory reactions, such as energy conversion, environmental remediation, and chemical transformation examples of reactions that require metal catalysis are pharmaceutical synthesis, chemical intermediates, agrochemicals, petroleum refining (Liu, et al., 2017). The catalytic activity of metals occurs at their surface; any metal atom/ion without interaction with the reactant particles is considered waste; therefore, to decrease the degree of waste, the use of metals as a catalyst with a high surface area to volume ratio is required. Metal nanoparticles are spread onto the surface of eco-friendly support with a high-surface area, are stable at high temperatures, and can prevent metal agglomerations during production and catalytic reaction. Therefore the reactant molecules can access as many surface atoms of the metal as possible due to their dispersion on support with a large surface area (Liu, et al., 2017). Various supports for transition metal catalysts improve their catalytic efficiency compared to unsupported catalysts due to the increase in active phase dispersion (Kambo et al., 2018).

When nanoparticles are distributed on large-surface-area supports, their interactions with the support surfaces become crucial in determining their catalytic efficiency (Massaro et al., 2017). The synthesis of various supports for metal nanoparticles such as carbon nanotubes (Fihri et al., 2011, Salvo et al., 2016), zeolite, dendrimers (Liu et al., 2016), titanium dioxide (Pires et al., 2015), alumina (Massaro et al., 2017), silica (Pavia et al., 2013), and other materials have received a lot

of attention. There have been reports of an increase in the degradation efficiency when transition metal catalysts are aided by carbon nanotubes (Chio et al., 2019, Ma et al., 2017). However, carbon nanotubes and zeolites have complex preparation methods and can be expensive. Furthermore, the structure of carbon nanotubes can disintegrate at a higher temperature, resulting in a small surface area (Mun & Horri, 2018). In contrast, clay minerals which include montmorillonite (lamellar), sepiolite (fibrous), kaolinite (lamellar), and halloysite nanotubes (tubular), occur naturally in a variety of shapes and sizes.

### **2.3.1 Factors Affecting Photocatalytic Activity**

Several factors affect photocatalyst performance during photocatalytic reactions as presented in Figure 2.2.

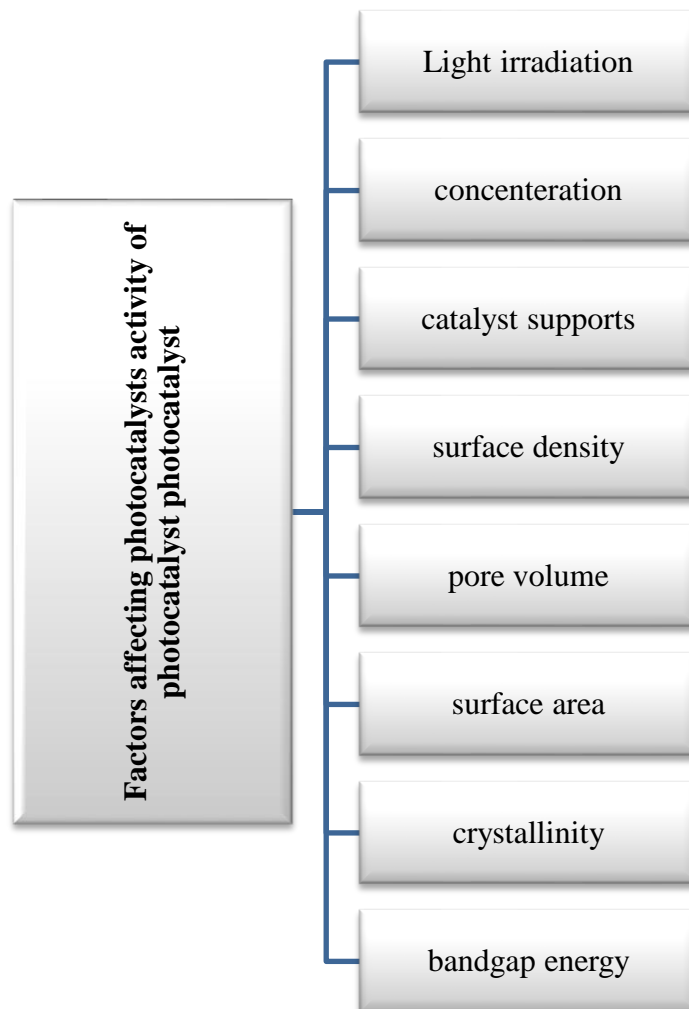


Figure 2.2 Factors affecting photocatalysts activity.

### 2.3.1(a) Light irradiation

The photocatalytic reaction's kinetics and quantum effectiveness are greatly influenced and enhanced by the light irradiation period, intensity, and wavelength (Dong et al., 2015). The photocatalytic degradation rate is proportional to the intensity of the light source (Jia et al., 2016). As the intensity of the light increases, the number of photons interacting with the surface area of semiconductors increases (Zare et al., 2021). The electrons in the valence band (VB) are stimulated to the conduction band (CB) when the photon energy is absorbed by the photocatalyst, generating electron/hole pairs (Chen et al., 2008). Increased intensity can speed up photocatalytic degradation

by increasing the chance of photocatalyst excitation (Saleh et al., 2011). In the photocatalysis process, electron-hole pair recombination is a well-known issue affecting the process. Photodegradation activity will be hampered by increased recombination rates and decreased electron/hole pair separation at lower light intensities, resulting in lesser photogeneration of free radicals (Gouthaman et al., 2018). The photocatalyst must be able to absorb the a large part of the visible spectrum to achieve very effective degrading performance. It has been observed that frequently used photocatalysts have a large band gap energy ( $E_g > 3.0$  eV), such as  $\text{TiO}_2$ ,  $\text{CuO}$ ,  $\text{SnO}_2$ ,  $\text{NiO}$ ,  $\text{Ag}_2\text{WO}_4$ ,  $\text{ZnO}$ , and others, and were found to be only effective in the UV region of the spectrum, absorbing just 5% of the visible spectrum at a wavelength ( $\lambda$ ) of  $<388$  nm (Kumar & Devi, 2011). Researchers have recently concentrated on using visible light to produce low-cost degradation processes. Unfortunately, most photocatalysts with a wide band gap energy are not active under visible light, which account for 43% and 52% of visible light, respectively (Liu et al., 2017).

### **2.3.1(b) Concentration**

The most significant parameter determining photocatalytic activity is the amount of active phase of the photocatalyst. Optimizing the number of active phases used throughout the photocatalytic process is important to minimize the waste of photocatalysts. A maximal efficiency with the lowest active phase concentration is required for the economic viability of photoreaction (Zare et al., 2021). The photocatalytic performance increases when the amount of photocatalyst is increased. This is because the number of active sites on the photocatalyst surface has increased. As a result, many hydroxyl radicals and other reactive oxygen species (ROS) will be produced, responsible for the actual degradation of organic compounds (Ammar et al., 2020). Even so, a higher amount of photocatalysts during photocatalytic reactions can result in decreasing light